Astronomy & Astrophysics

Testing for redshift evolution of Type Ia supernovae using the strongly lensed PS1-10afx at *z* = 1.4

T. Petrushevska[1], R. Amanullah[1], M. Bulla[1], M. Kromer[2,3], R. Ferretti[1], A. Goobar[1], and S. Papadogiannakis[1]

[1] Oskar Klein Centre, Department of Physics, Stockholm University, 106 91 Stockholm, Sweden
e-mail: tpetr@fysik.su.se
[2] Zentrum für Astronomie der Universität Heidelberg, Institut für Theoretische Astrophysik, Philosophenweg 12, 69120 Heidelberg, Germany
[3] Heidelberger Institut für Theoretische Studien, Schloss-Wolfsbrunnenweg 35, 69118 Heidelberg, Germany

ABSTRACT

Context. The light from distant supernovae (SNe) can be magnified through gravitational lensing when a foreground galaxy is located along the line of sight. This line-up allows for detailed studies of SNe at high redshift that otherwise would not be possible. Spectroscopic observations of lensed high-redshift Type Ia supernovae (SNe Ia) are of particular interest since they can be used to test for evolution of their intrinsic properties. The use of SNe Ia for probing the cosmic expansion history has proven to be an extremely powerful method for measuring cosmological parameters. However, if systematic redshift-dependent properties are found, their usefulness for future surveys could be challenged.
Aims. We investigate whether the spectroscopic properties of the strongly lensed and very distant SN Ia PS1-10afx at $z = 1.4$, deviates from the well-studied populations of normal SNe Ia at nearby or intermediate distance.
Methods. We created median spectra from nearby and intermediate-redshift spectroscopically normal SNe Ia from the literature at -5 and $+1$ days from light-curve maximum. We then compared these median spectra to those of PS1-10afx.
Results. We do not find signs of spectral evolution in PS1-10afx. The observed deviation between PS1-10afx and the median templates are within what is found for SNe at low and intermediate redshift. There is a noticeable broad feature centred at $\lambda \sim 3500$ Å, which is present only to a lesser extent in individual low- and intermediate-redshift SN Ia spectra. From a comparison with a recently developed explosion model, we find this feature to be dominated by iron peak elements, in particular, singly ionized cobalt and chromium.

Key words. supernovae: individual: PS1-10afx – gravitational lensing: strong – supernovae: general

1. Introduction

Type Ia supernovae (SNe Ia) have proven to be extremely powerful for studying the nature of the accelerated expansion of the Universe (see e.g. Goobar & Leibundgut 2011, for a review). Although Einstein's cosmological constant is not challenged by the latest results (Betoule et al. 2014), it is not unproblematic, and there is a rich choice of alternative explanations that are also consistent with the current data (Dhawan et al. 2017). These are best addressed with high-quality data at high redshift. At present, the sample of SNe Ia at $z \geq 1$ is still small and mostly provided by the *Hubble* Space Telescope (HST, Riess et al. 2007; Suzuki et al. 2012; Rodney et al. 2012; Rubin et al. 2013). This will improve with future space-based surveys such as the Wide Field Infrared Survey Telescope (WFIRST; Spergel et al. 2015) and possibly EUCLID (Astier et al. 2014). For example, WFIRST is expected to detect ~2700 SNe Ia up to $z \approx 1.7$ and will be limited by systematic errors (Spergel et al. 2015). One important systematic effect is the possibility that the mean SN properties evolve with redshift in a way that cannot be corrected with the current standardization techniques (Howell et al. 2007; Foley et al. 2008a; Sullivan et al. 2010).

Properties of galaxies such as mass, age, dust and metallicity change with cosmic time, and this may also affect the SNe that they host. In order to test for systematic variations of the SN Ia population with time, mean spectra at low, intermediate and high redshift have been constructed to measure the possible evolution of SN Ia spectral properties (Ellis et al. 2008; Sullivan et al. 2009; Foley et al. 2012b; Maguire et al. 2012). These studies did not find any change in the optical part, while the near-UV showed increased scatter. In particular, Maguire et al. (2012) detected a ~3σ excess of the pseudo-continuum flux for the intermediate-redshift mean spectrum compared to the nearby one. Sullivan et al. (2009) found a slight decrease with redshift in the strength of intermediate-mass element features (Si II, Ca II, and Mg II), but concluded that this is not an evolutionary effect of intrinsic SN properties.

While the large diversity of SNe Ia in the UV domain is supported by some theoretical studies that predict sensitivity to differences in explosion mechanisms, progenitor age, metallicity and environment, it is not certain which of these play the dominant role (see e.g. Parrent et al. 2014). For instance, Timmes et al. (2003) studied the production of ^{56}Ni in relation to the initial metallicity of the progenitor white dwarf. The reasoning behind this is that the presence of metals in the white dwarf translates into lower proton-to-nucleon ratios, which leads to the production of more neutron-rich nuclei of the iron group elements (IGEs) and less radioactive ^{56}Ni (Höflich et al. 1998). Since UV spectra are characterized by strong line-blanketing from IGE lines, higher (lower) UV fluxes are typically expected for lower (higher) progenitor metallicities (Lentz et al. 2000). However, despite these efforts, there is no consensus yet regarding the relationship between progenitor metallicity and SN spectra.

At present, the signal-to-noise ratio (S/N) and the resolution of the high-z sample spectra from HST (Riess et al. 2007) is not good enough for a detailed study. Thus, even individual high S/N events at high redshift could be of interest if they show discrepancies from what has been observed in the large low-z samples. This unique opportunity arose with the discovery of the strongly lensed SN Ia PS1-10afx. Here, we analyse this first high-S/N rest-frame near-UV SN Ia spectrum. Another magnified SN Ia dubbed SN HFF14Tom at $z = 1.3457$ was found behind a galaxy cluster (Rodney et al. 2015), but because of the modest magnification, it had a lower S/N and is therefore not considered in this work.

The source PS1-10afx was discovered on 2010 August 31.35 UT with the 1.8 m Pan-STARSS1 (PS1) telescope as part of the PS1 Medium Deep Survey. Follow-up observations and near-infrared (NIR) spectroscopy revealed a redshift of $z = 1.3883$. Based on the redshift, the transient was brighter than any previously observed SN. Therefore, Chornock et al. (2013, C13) classified PS1-10afx as a new type of superluminous SN, but the shape of the light curve did not fit those expected for superluminous SNe well. Later, Quimby et al. (2013) classified PS1-10afx as an SN Ia magnified ~30 times. This magnification was caused by a galaxy lens whose redshift was determined from the Mg II and Ca II in the Keck/LRIS spectrum taken three years after the SN explosion (Quimby et al. 2014, Q14).

2. Analysis

In this work we make use of three of the spectra presented in C13 obtained with ground-based facilities. There are two GMOS-S and GMOS-N optical (observer frame) spectra, and one FIRE/Magellan NIR observer frame spectrum. The optical spectra are at phase of −5.0 and +1.2 d with respect to the B-band maximum rest-frame epoch, while the NIR spectrum is from −2.1 d[1]. The PS1-10afx spectra have been corrected for Galactic extinction $E(B-V) = 0.05$ mag (Schlafly & Finkbeiner 2011). Since the observed SN colours suggest no extinction (Q14), no de-reddening to correct for host extinction was applied. We did, however, detect interstellar Mg II absorption at 2796 Å and 2804 Å at the host galaxy redshift, which according to the empirical relation found by Ménard et al. (2008) would indicate non-negligible extinction. However, as shown in Amanullah et al. (2015), reddening of SNe Ia correlates very poorly with Mg II absorption.

The Si II 6355 Å feature is typically used to classify SNe Ia. As discussed in Quimby et al. (2013), this feature is not prominent in the optical rest-frame spectrum, although this is uncertain because of the low S/N in the red part of the spectrum (see also Sect. 3). There are peculiar SN Ia subtypes where this feature is weak (1999aa-like, see e.g. Garavini et al. 2004) or even almost completely absent (1991T-like SNe Ia, see Filippenko et al. 1992). However, 1999aa- and 1991T-like SNe Ia have slower decline rates with $\Delta m_{15}(B) \lesssim 0.9$ mag, in contrast with PS1-10afx that has $\Delta m_{15}(B) = 1.22 \pm 0.09$. Moreover, they are known to have bluer UV colour evolution than normal SNe Ia (Brown et al. 2014; Smitka et al. 2015). The comparison of the light-curve shapes and UV rest-frame colours predicted from the SN Ia templates in Quimby et al. (2013) further confirms PS1-10afx as a normal SN Ia.

Table 1. PS1-10afx Ca II H&K feature properties.

Spectrum phase	$v_{\text{Ca II}}$ (10^3 km s^{-1})	$pEW_{\text{Ca II}}$ (Å)
−5.0 d	16.5 (2.8)	88 (8)
−2.1 d	16.7 (3.0)	103 (13)
+1.2 d	16.0 (3.0)	75 (19)

Notes. Uncertainties are given in parentheses.

2.1. Velocity and pEW of the Ca II H&K feature

First, we focus on the prominent SN absorption feature at ~3700 Å, to which Ca II H&K, Si II and various ionization states of the iron-peak elements contribute significantly. The Ca II H&K feature strength, expressed as pseudo-equivalent width (pEW), and the line blue-shift with respect to the rest wavelength of 3945.12 Å, expressed as expansion velocity, have previously been used as a diagnostic for SN Ia evolution. Garavini et al. (2007) measured Ca II H&K expansion velocities and pEWs for 13 SNe Ia at $0.279 < z < 0.912$, and concluded that they did not deviate significantly from the nearby SNe Ia.

We measured the expansion velocities and pEWs for PS1-10afx and the results are shown in Table 1. The large uncertainties in the velocity measurements are due to the overlapping [O II] emission line. The given errors represent the two extreme values of the velocity when we assume that the minimum of the Ca II H&K feature is at either side of the host galaxy emission line. We measure an expansion velocity of ~16 500 km s^{-2}, consistent with the value previously reported by C13, and a pEW at maximum of ~80 Å. The mean value of the Ca II H&K velocity in the Folatelli et al. (2013) nearby sample is ~15 000 ± 3000 km s^{-1} and pEW of ~120 ± 30 Å, measured around B-band maximum brightness. With their large uncertainties, the values for PS1-10afx are statistically consistent with the nearby sample.

2.2. Spectral comparisons

Space-based facilities such as HST and the *Swift* satellite, have allowed studies of nearby SNe Ia in the UV (see e.g. Brown et al. 2014). We can use the spectroscopically normal SNe Ia from this sample at similar phase with PS1-10afx to make a comparison. As SN Ia spectra evolve rapidly, particularly in the UV (see e.g. Hook et al. 2005), we restrict the epochs of the nearby UV spectra to phases within ±2.5 d from the PS1-10afx epochs. First, we use the optical spectrum at −5.0 d, since it has the highest S/N. At phases −7.5 to −2.5 d, we found eight SNe from the literature and their properties are shown in Table 2. SN 2014J also meets the criteria, but since it is highly reddened by its host galaxy (e.g. Goobar et al. 2014; Amanullah et al. 2014), it was not included in this analysis. We used the *Swift* spectra that have been re-reduced by Smitka et al. (2016) with their novel decontamination technique. The spectra were corrected for Galactic and host extinction. We used the parameterization of Milky Way extinction from Fitzpatrick (1999) and $R_V = 3.1$. Following previous studies with SN Ia UV spectra (Foley et al. 2016), the spectra were normalised with a top-hat passband at $\lambda \sim 4000$ Å. When two spectra were close to the required phase, we took the average to give a mean phase of −5.0 d. In Fig. 1 we show the comparison between the early PS1-10afx spectrum and the low-z SN Ia sample.
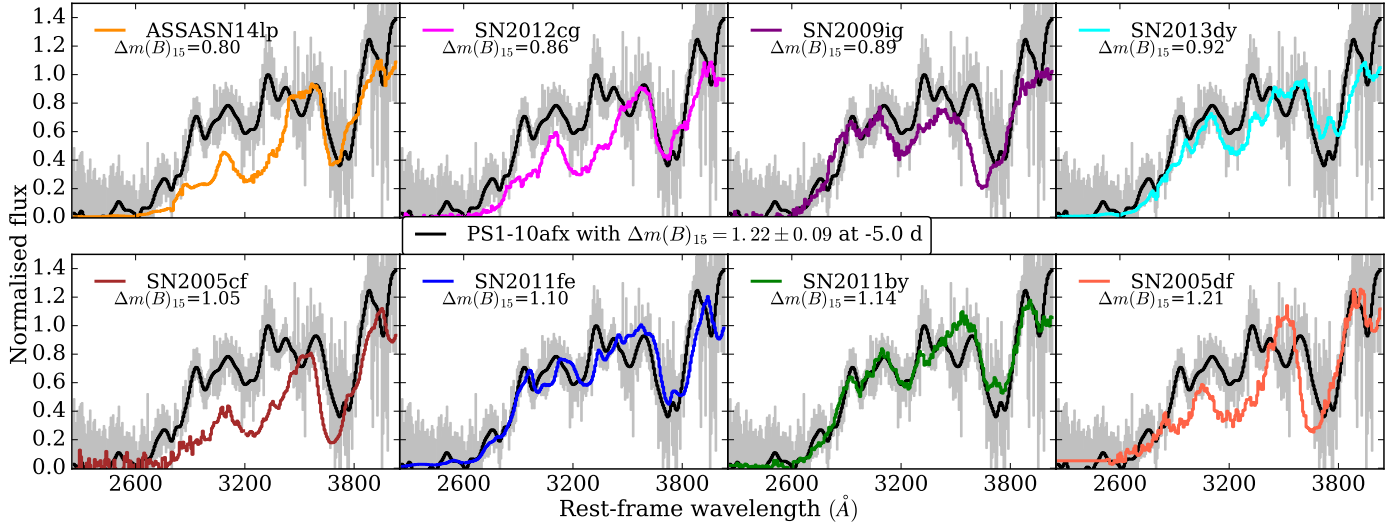
---

[1] There is also one NIR spectrum at phase +2.0 d, but because of the low S/N and limited wavelength coverage it is not used in this study.

Fig. 1. PS1-10afx at phase -5.0 d (grey line) and nearby SN Ia spectra at similar phases. When there were two spectra close to the required phase, we took the average. The black line shows the PS1-10afx spectrum rebinned by a factor of 10. The spectra were normalised at ~4000 Å. The nearby spectra are ordered according to their light-curve shape parameter $\Delta m_{15}(B)$.

Table 2. Properties of the nearby SNe Ia used for the early-time (-5 d) median spectrum.

SN name	ASASSN-14lp	SN 2012cg	SN 2009ig	SN 2013dy	SN 2005cf	SN 2011fe	SN 2011by	SN 2005df
z_{helio}	0.005101^a	0.001447^c	0.007589^c	0.00383^g	0.006^h	0.002000^j	0.002843^c	0.004350^n
A_V	0.99^a	0.34^d	0.01^f	0.64^g	0.10^h	0.08^j	0.03^l	0.001^n
MW A_V	0.0682	0.0558^d	0.088^f	0.46^g	0.269^h	0.024^j	0.038^l	0.090^n
$\Delta m_{15}(B)$	$0.80(0.05)^a$	$0.86(0.02)^d$	$0.89(0.02)^f$	$0.92(0.03)^g$	$1.05(0.03)^h$	$1.10(0.04)^j$	$1.14(0.03)^m$	$1.21(0.04)^n$
instr.	STIS/HST^b	*Swift^e*	*Swift^e*	STIS/HST^g	*Swift^i*	STIS/HST^k	*Swift^e*	*Swift^e*
sp. phase	-4.4 d^b	-7.2 d^e	-4.2 d^e	-6.6 -2.5 d^g	-5.8 d^i	-6.9 -2.9 d^j	-7.9 -3.9 d^e	-5.2 d^e

Notes. Uncertainties of the light-curve shape parameter $\Delta m_{15}(B)$ are given in parentheses.

References. [a] Shappee et al. (2016); [b] Foley et al. (2016); [c] From NED; [d] Marion et al. (2016); [e] Smitka et al. (2016); [f] Foley et al. (2012a); [g] Pan et al. (2015); [h] Wang et al. (2009); [i] Bufano et al. (2009); [j] Pereira et al. (2013); [k] Mazzali et al. (2014); [l] Graham et al. (2015); [m] Silverman et al. (2013); [n] Milne et al. (2010).

There is no perfect agreement to PS1-10afx with any of the observed nearby objects. However, the shape of the continuum and most of the features agree well with those of the spectra of SN 2011fe, 2011by and 2013dy. In contrast, the blue component of the Ca II H&K feature in SN 2009ig, SN 2005cf and SN 2005df differs from that of PS1-10afx. It has been proposed that the blue component is caused by either high-velocity calcium or Si II 3859 Å (Foley 2013, and references therein).

In Fig. 1 we order the nearby SN spectra according to their light-curve shape parameter Δm_{15}, motivated by Foley et al. (2008a, 2016), who argued that the UV spectral continuum is driven primarily by this parameter. In particular, Foley et al. (2016), after normalising at ~4000 Å, found that SNe with lower values of Δm_{15} have a higher flux level at ~3000 Å. However, in the limited range of Δm_{15} values from 0.8 to 1.2, which our sample spans, this correlation is not obvious. However, we do find that the flux at ~3025 Å is between ~35 and 65% of that at ~4000 Å. Although our spectra are at earlier epochs than those of Foley et al. (2016), the flux ratio that we measure is consistent with their findings (upper left panel of their Fig. 3).

Using published data of normal nearby SNe Ia, we also constructed median spectra at phases similar to those of PS1-10afx. When building the median spectrum, we used the same restriction on phase and normalisation as outlined above. At phases

close to -5 d, we used the SNe Ia in Table 2 and shown in Fig. 1, while at phases close to $+1.2$ d, we also found eight SNe that are in the appropriate range, and we list them in Table 3. In the upper panels of Figs. 2 and 3 we compare the median spectra with the rms scatter at low redshift with spectra of PS1-10afx at -5 d and $+1.2$ d, respectively. To illustrate how much PS1-10afx differs from the median spectra, we also plot the pull values (i.e. the residuals divided by the square root of rms squared) in the lowest panel. In order to assess the significance of the observed deviations, we also applied a jack-knife approach for the nearby sample. The median spectrum was constructed after leaving out one of nearby spectra at the time. This spectrum is then compared to the median spectrum in the same manner as for PS1-10afx. The result is shown in Fig. 4, from which we can conclude that the deviations of PS1-10afx are similar to the results from the jack-knife exercise, and all pulls are within 3 at all wavelengths.

We also compared PS1-10afx with median spectra at intermediate redshift. Ellis et al. (2008) used the LRIS/Keck to observe a homogeneous sample of 36 SNe Ia at $0.1 < z < 0.8$ discovered with the Canada-France-Hawaii Telescope Supernova Legacy Survey (Astier et al. 2006; SNLS). From these host-subtracted spectra, we constructed one median spectrum at phase -5.0 d and another at $+1.2$ d, with the same requirement for the spectra phases as for low redshift. For the early median spectrum, 9 spectra satisfy the requirement and their mean redshift

Table 3. Properties of the nearby SNe Ia used for the median spectrum at phase +1.2 d.

SN name	SN 2009ig	SN 2013dy	SN 1981B	SN 2001ba	SN 2011fe	SN 2011by	SN 2005df	SN 1992A
z_{helio}	0.007589	0.00383	0.005101^c	0.029557^c	0.002000	0.002843	0.004350	0.001447^c
A_V	0.01	0.15	0.35^d	0.016^d	0.08	0.03	0.001	0.016^d
MW A_V	0.088	0.92	0.0682^d	0.176^d	0.024	0.038	0.090	0.046^d
$\Delta m_{15}(B)$	0.89(0.02)	0.92(0.03)	$1.01(0.10)^d$	$1.01(0.11)^d$	1.10(0.04)	1.14(0.03)	1.21(0.04)	$1.47(0.11)^d$
instr.	$Swift^a$	$STIS/HST^b$	IUE^d	$STIS/HST^d$	$Swift^a$	$Swift^a$	$Swift^a$	IUE^d
sp. phase	$+1.6^a$	$+1.2\ \text{d}^b$	$+1.8\ \text{d}^d$	$+3.8\ \text{d}^d$	$+0.1\ +3.0\ \text{d}^a$	$+1.1\ \text{d}^a$	$+1.6\ \text{d}^a$	$-0.2\ +2.4\ \text{d}^d$

Notes. Uncertainties of the light-curve shape parameter $\Delta m_{15}(B)$ are given in parentheses.
References. $^{(a)}$ Smitka et al. (2016); $^{(b)}$ Pan et al. (2015) ; $^{(c)}$ From NED; $^{(d)}$ Foley et al. (2008b).
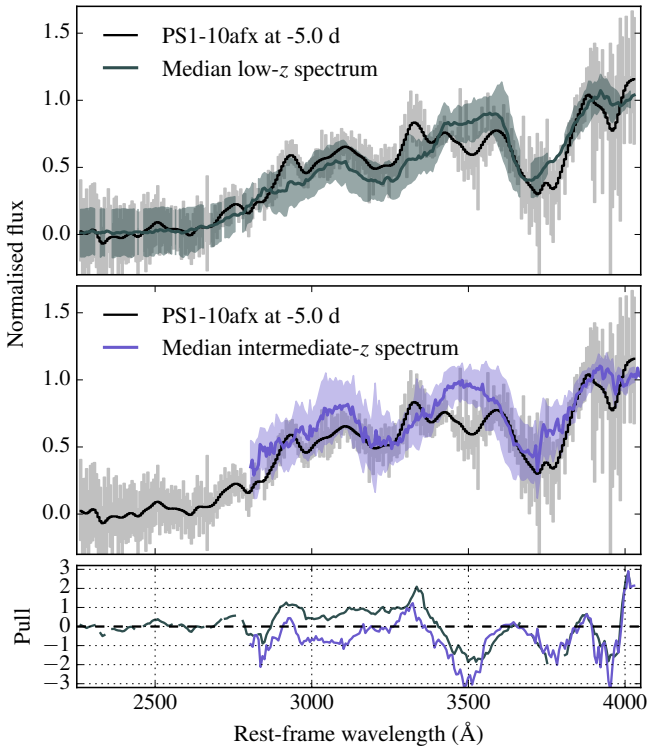

Fig. 2. PS1-10afx at -5.0 d compared with low- and intermediate-redshift median spectra constructed from normal SNe Ia at similar phases. The spectra were normalised at $\sim$4000 Å. The shaded regions represent the root mean square of the sample in green and blue for the nearby and intermediate SNe Ia, respectively. *The lower panel* shows the pull for the low- (green) and intermediate-redshift (blue) spectrum.
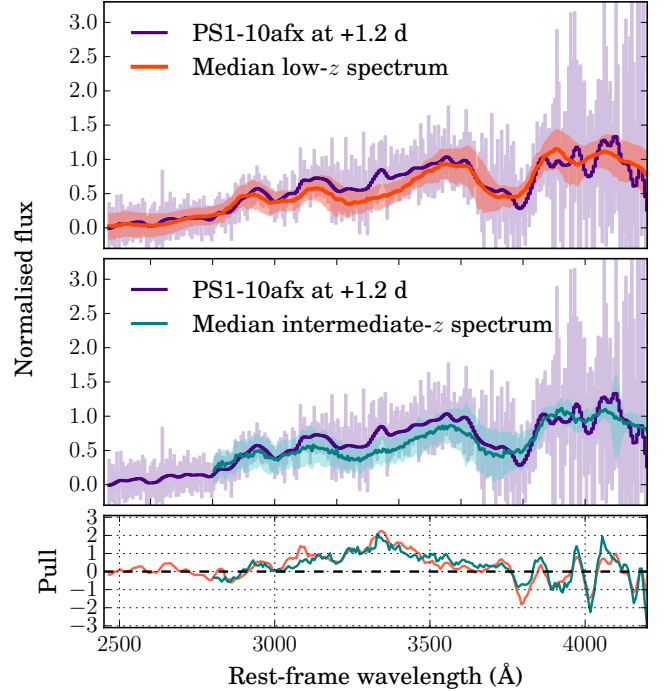

Fig. 3. PS1-10afx at +1.2 d compared with low- and intermediate-redshift median spectra constructed from normal SNe Ia at similar phases. The shaded regions represent the root mean square of the sample in pink and cyan for the nearby and intermediate SNe Ia, respectively. The lower panel shows the pull for the low- (pink) and intermediate-redshift (cyan) spectrum.

is $z_{\text{mean}} = 0.44$. For the median spectrum at +1.2 d, 11 spectra satisfy the requirement and their mean redshift is $z_{\text{mean}} = 0.46$. The comparison of the early and maximum PS1-10afx spectra to the median intermediate-z spectra is shown in the middle panels in Figs. 2 and 3. The intermediate-redshift templates look similar to their low-redshift counterparts, with some discrepancies at $\lambda < 3000$ Å, consistent with previous results (Sullivan et al. 2009; Maguire et al. 2012).

The agreement of the PS1-10afx spectra with the SN Ia templates is good, within the range of variability of the nearby and intermediate sample which is less than 3σ. We discuss the largest discrepancy that we find in the following section.

3. Discussion

The PS1-10afx spectra are statistically consistent with the diversity seen in nearby and intermediate-redshift observations at comparable epochs, despite the modest size of the samples.

We note that the early PS1-10afx spectrum shows an extended feature in the region centred at $\lambda \sim 3500$ Å. This feature is also observed in SN Ia spectra and is present to a lesser extent in some of the individual spectra that make up the median low- and intermediate-redshift spectra, for instance in SN 2013dy (see Fig. 1). The lensed SN Ia, SN HFF14Tom at $z = 1.3457$, can be matched with nearby normal SNe Ia (Rodney et al. 2015) and is broadly consistent with PS1-10afx. However, SN HFF14Tom did not exhibit a similar feature at $\lambda \sim 3500$ Å, although this is uncertain as it could have been lost in the low S/N. The difference between the spectra of PS1-10afx and SN 2011fe over the range of 3300–3700 Å appears to have an $EW \sim 40$ Å. The interstellar Ca ɪɪ H&K absorption lines of the lensing galaxy fall in this region, as reported by Q14. However, the interstellar medium (ISM) lines can have an EW of at most a few Å and only contribute a small amount ($<10\%$) to the observed difference between the spectra. Furthermore, the feature spans $\sim$200 Å of the spectrum. Given the resolution of
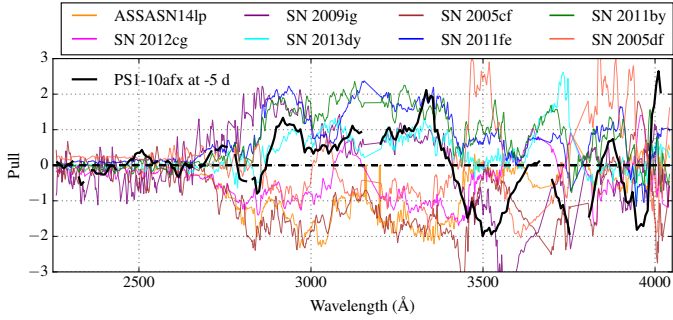
Fig. 4. Pull of PS1-10afx at -5.0 d compared with the low-redshift median spectrum constructed from all the SNe Ia in Table 2, shown by the black line. The coloured lines represent the pulls of the individual nearby SNe Ia compared to the median spectrum constructed by leaving that one out from all the SNe Ia spectra.
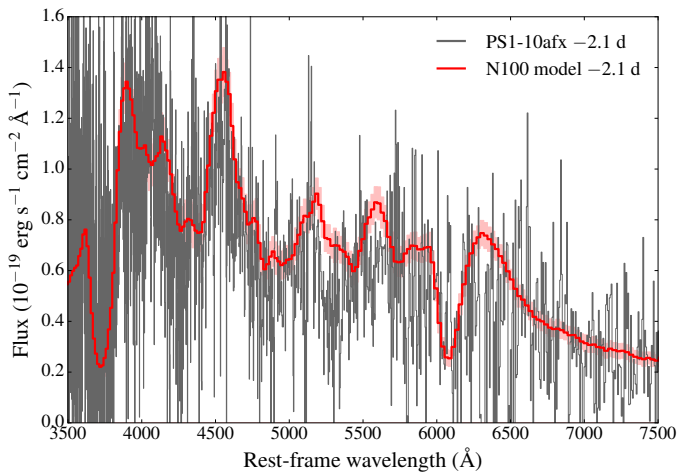

Fig. 5. Comparison between the optical spectrum of PS1-10afx and the spectrum predicted by the N100 model of Seitenzahl et al. (2013). Unlike Figs. 1–4, absolute fluxes are reported here. The observed spectrum is shown in grey and has been demagnified assuming $\mu = 30.8$ from Quimby et al. (2013). An angle-averaged spectrum for the three-dimensional N100 model is shown in red, while light red regions show the dispersion that is due to viewing-angle effects.

the spectrum, the ISM lines of the lensing galaxy will have a FWHM of $\sim$10 Å and be separated by $\sim$30 Å at the host galaxy rest frame. This suggests that the profile of the feature is intrinsic to the SN itself.

To investigate the nature of this feature, we examined the near-UV spectrum predictions from a recently developed multidimensional explosion model. Specifically, for our comparison we selected the three-dimensional N100 model (Röpke et al. 2012; Seitenzahl et al. 2013). This model describes the thermonuclear explosion of a carbon-oxygen white dwarf at the Chandrasekhar mass limit and is found to reproduce observables of normal SNe Ia in the optical reasonably well (Röpke et al. 2012; Sim et al. 2013; Bulla et al. 2016).

Figure 5 shows a comparison between the optical spectrum of PS1-10afx at -2.1 d relative to maximum and the spectrum predicted by the N100 model at the same epoch. The flux spectrum of PS1-10afx has been demagnified assuming a magnification factor of $\mu = 30.8^{+5.6}_{-4.8}$ (Quimby et al. 2013), while the model spectrum has been scaled to the distance of PS1-10afx. Although the S/N in the observations prevents us from investigating individual features in great detail, we note a good match between model and data in both luminosity and overall spectral
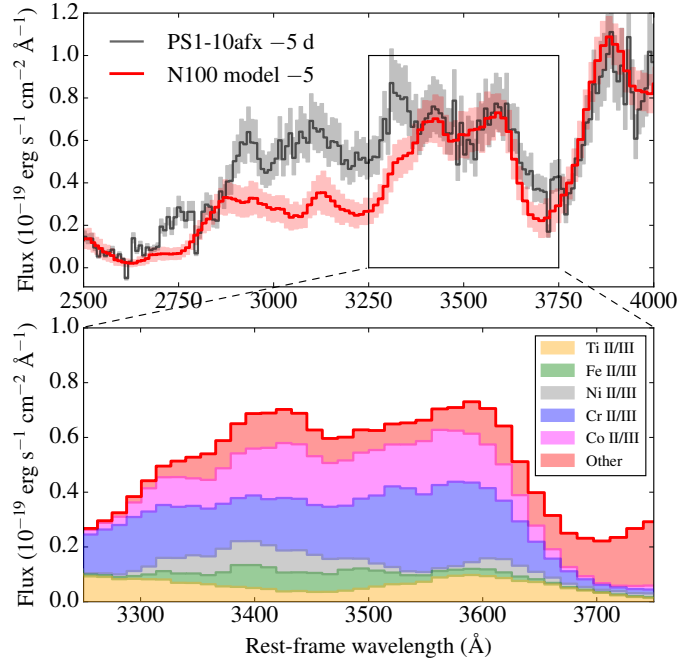

Fig. 6. *Upper panel*: same as Fig. 5, but in the near-UV. The observed spectrum was rebinned by a factor of 15 to have a similar bin size ($\sim$10 Å) as in the model spectrum. *Bottom panel*: zoom of the N100 model into the spectral region around 3500 Å. The region below the total flux (red line) is colour-coded to indicate the relative contributions of different element transitions.

shape. The top panel of Fig. 6 shows the near-UV spectrum of PS1-10afx at -5 d relative to maximum compared to the synthetic spectrum of the N100 model at the same epoch. The absolute fluxes are scaled as described above. We note a reasonable match between synthetic and observed spectra (but see below) not only in terms of the overall spectral shape but also across individual spectral features (see e.g. the Ca II H&K line). In particular, the N100 model predicts a feature in the wavelength region around 3500 Å, with both line strength and width comparable to those observed in PS1-10afx. As shown in the bottom panel of Fig. 6, the spectral region between $\sim$3300 and 3600 Å is dominated by transitions from iron-group elements. Specifically, the characteristic feature around 3500 Å appears to originate mostly from singly and doubly ionized Co and Cr transitions.

We note that the model predicts flux at wavelengths shorter than 3400 Å that is lower than the early near-UV PS1-10afx spectrum. We caution that absolute comparison studies for lensed SNe are not straightforward as their absolute flux depends on the exact magnification factor assumed. Nevertheless, one intriguing possibility is that the flux difference observed in the near-UV might be due in part to metallicity effects. The initial carbon-oxygen white dwarf in the N100 model of Seitenzahl et al. (2013) contains 2.5% of ^{22}Ne to mimic the effects of a solar metallicity zero-age main-sequence progenitor star on the nuclear burning. Thus, it is tempting to think that lower progenitor metallicities might result in higher UV fluxes and thus provide better agreement with PS1-10afx. Q14 found the best-fit value of PS1-10afx host to be $\sim$0.4 times the solar metallicity, supporting this possibility. We note, however, that Seitenzahl et al. (2013) did not include IGEs in solar composition in their progenitor models, which could significantly affect the predicted UV spectra.

Although Seitenzahl et al. (2013) computed alternative versions of the N100 models with different metallicities, no

radiative transfer calculations have been performed for these models and it is thus unclear to which extent metallicity would affect the UV and optical part of the spectrum. In an earlier work using the one-dimensional W7 model (Nomoto et al. 1984; Thielemann et al. 1986), Lentz et al. (2000) studied the impact of a wide range of progenitor metallicities on the observed spectra. In their Fig. 9, the 3500 Å feature is also visible and its strength depends on the assumed metallicity, although there is no simple linear relation between the feature strength and the metallicity. In addition, metallicities of well-studied nearby SN Ia host galaxies show a great range of variation (Zahid et al. 2012), thus the metallicity measured for PS1-10afx host is not exceptional. In conclusion, PS1-10afx does not show signs of evolution, and this is in agreement with the sample of nearby normal SNe Ia.

4. Summary and conclusions

We have compared the spectra of a magnified high-redshift SN Ia at $z = 1.4$ and spectra compiled from nearby and intermediate-redshift normal SNe Ia. Comparing rest-frame wavelengths from 2500 to 4000 Å, we found PS1-10afx to be in good ($<3\sigma$) agreement with the nearby sample. We used the spectral time series to measure the pEW and velocity and found them to be statistically consistent with those for nearby observations. From this comparison, there is no statistically significant evidence that this SN Ia exhibits a redshift evolution. The spectrum of PS1-10afx at -5.0 d shows a broad feature at $\lambda \sim 3500$ Å, which is only mildly present in nearby and intermediate-redshift SNe Ia. Because this feature is dominated by IGEs, it seems possible that metallicity effects could play a role in this difference. However, with the current uncertainties of both models and data, it is not possible to place any firm constraints.

In the second half of the 2020s, the wide-field space-based SN survey, WFIRST, will provide numerous SN Ia light curves at high-z to be used for cosmological studies, thus systematic uncertainties are expected to limit the accuracy in the measurements of cosmological parameters. The possible evolution of SN Ia properties with redshift could contribute significantly to the systematic error budget. With PS1-10afx, we were able to test this possibility several years before planned SN surveys come online. As the study done here is limited to one SN Ia, it is quite possible that not all SNe Ia at $z \sim 1.4$ are represented by PS1-10afx, thus that all high-z are similar to the normal nearby SNe Ia Furthermore, we emphasize that even though PS1-10afx is consistent with low- and intermediate-z data, this does not prove that the average SED does not evolve with redshift. However, spectroscopically normal SNe Ia must be present in the high-redshift Universe, so the effort of the future surveys consist of selecting these events as early as possible from the light curves in time to ask for a follow-up spectrum.

Our study was made possible thanks to the magnification from the foreground lens galaxy, otherwise PS1-10afx would have been undetected. Wide-field ground-based surveys will see first light very soon, the Zwicky Transient Facility in 2018 (ZTF; Kulkarni 2016) and the Large Synoptic Survey Telescope in 2021 (LSST; LSST Science Collaboration et al. 2009). So far, we have witnessed only two strongly lensed and magnified SNe Ia, PS1-10afx and iPTF16geu (Goobar et al. 2017). We expect that the number will increase after these wide-field ground-based surveys come online (Goldstein & Nugent 2017). These new strongly lensed SNe Ia at high-z can be useful for similar studies as made here, before the launch of WFIRST.

References

Amanullah, R., Goobar, A., Johansson, J., et al. 2014, ApJ, 788, L21
Amanullah, R., Johansson, J., Goobar, A., et al. 2015, MNRAS, 453, 3300
Astier, P., Guy, J., Regnault, N., et al. 2006, A&A, 447, 31
Astier, P., Balland, C., Brescia, M., et al. 2014, A&A, 572, A80
Betoule, M., Kessler, R., Guy, J., et al. 2014, A&A, 568, A22
Brown, P. J., Kuin, P., Scalzo, R., et al. 2014, ApJ, 787, 29
Bufano, F., Immler, S., Turatto, M., et al. 2009, ApJ, 700, 1456
Bulla, M., Sim, S. A., Kromer, M., et al. 2016, MNRAS, 462, 1039
Chornock, R., Berger, E., Rest, A., et al. 2013, ApJ, 767, 162
Dhawan, S., Goobar, A., Mörtsell, E., Amanullah, R., & Feindt, U. 2017, JCAP, submitted [arXiv:1705.05768]
Ellis, R. S., Sullivan, M., Nugent, P. E., et al. 2008, ApJ, 674, 51
Filippenko, A. V., Richmond, M. W., Matheson, T., et al. 1992, ApJ, 384, L15
Fitzpatrick, E. L. 1999, PASP, 111, 63
Folatelli, G., Morrell, N., Phillips, M. M., et al. 2013, ApJ, 773, 53
Foley, R. J. 2013, MNRAS, 435, 273
Foley, R. J., Filippenko, A. V., Aguilera, C., et al. 2008a, ApJ, 684, 68
Foley, R. J., Filippenko, A. V., & Jha, S. W. 2008b, ApJ, 686, 117
Foley, R. J., Challis, P. J., Filippenko, A. V., et al. 2012a, ApJ, 744, 38
Foley, R. J., Filippenko, A. V., Kessler, R., et al. 2012b, AJ, 143, 113
Foley, R. J., Pan, Y.-C., Brown, P., et al. 2016, MNRAS, 461, 1308
Garavini, G., Folatelli, G., Goobar, A., et al. 2004, AJ, 128, 387
Garavini, G., Folatelli, G., Nobili, S., et al. 2007, A&A, 470, 411
Goldstein, D. A., & Nugent, P. E. 2017, ApJ, 834, L5
Goobar, A., & Leibundgut, B. 2011, Ann. Rev. Nuc. Part. Sci., 61, 251
Goobar, A., Johansson, J., Amanullah, R., et al. 2014, ApJ, 784, L12
Goobar, A., Amanullah, R., Kulkarni, S. R., et al. 2017, Science, 356, 291
Graham, M. L., Foley, R. J., Zheng, W., et al. 2015, MNRAS, 446, 2073
Höflich, P., Wheeler, J. C., & Thielemann, F. K. 1998, ApJ, 495, 617
Hook, I. M., Howell, D. A., Aldering, G., et al. 2005, AJ, 130, 2788
Howell, D. A., Sullivan, M., Conley, A., & Carlberg, R. 2007, ApJ, 667, L37
Kulkarni, S. R. 2016, in A$AS Meeting Abstracts, 227, 314.01
Lentz, E. J., Baron, E., Branch, D., Hauschildt, P. H., & Nugent, P. E. 2000, ApJ, 530, 966
LSST Science Collaboration 2009, ArXiv e-prints [arXiv:0912.0201]
Maguire, K., Sullivan, M., Ellis, R. S., et al. 2012, MNRAS, 426, 2359
Marion, G. H., Brown, P. J., Vinkó, J., et al. 2016, ApJ, 820, 92
Mazzali, P. A., Sullivan, M., Hachinger, S., et al. 2014, MNRAS, 439, 1959
Ménard, B., Nestor, D., Turnshek, D., et al. 2008, MNRAS, 385, 1053
Milne, P. A., Brown, P. J., Roming, P. W. A., et al. 2010, ApJ, 721, 1627
Nomoto, K., Thielemann, F.-K., & Yokoi, K. 1984, ApJ, 286, 644
Pan, Y. C., Foley, R. J., Kromer, M., et al. 2015, MNRAS, 452, 4307
Parrent, J., Friesen, B., & Parthasarathy, M. 2014, Ap&SS, 351, 1
Pereira, R., Thomas, R. C., Aldering, G., et al. 2013, A&A, 554, A27
Quimby, R. M., Werner, M. C., Oguri, M., et al. 2013, ApJ, 768, L20
Quimby, R. M., Oguri, M., More, A., et al. 2014, Science, 344, 396
Riess, A. G., Strolger, L.-G., Casertano, S., et al. 2007, ApJ, 659, 98
Rodney, S. A., Riess, A. G., Dahlen, T., et al. 2012, ApJ, 746, 5
Rodney, S. A., Patel, B., Scolnic, D., et al. 2015, ApJ, 811, 70
Röpke, F. K., Kromer, M., Seitenzahl, I. R., et al. 2012, ApJ, 750, L19
Rubin, D., Knop, R. A., Rykoff, E., et al. 2013, ApJ, 763, 35
Schlafly, E. F., & Finkbeiner, D. P. 2011, ApJ, 737, 103
Seitenzahl, I. R., Ciaraldi-Schoolmann, F., Röpke, F. K., et al. 2013, MNRAS, 429, 1156
Shappee, B. J., Piro, A. L., Holoien, T. W.-S., et al. 2016, ApJ, 826, 144
Silverman, J. M., Ganeshalingam, M., & Filippenko, A. V. 2013, MNRAS, 430, 1030
Sim, S. A., Seitenzahl, I. R., Kromer, M., et al. 2013, MNRAS, 436, 333
Smitka, M. T., Brown, P. J., Suntzeff, N. B., et al. 2015, ApJ, 813, 30
Smitka, M. T., Brown, P. J., Kuin, P., & Suntzeff, N. B. 2016, PASP, 128, 034501
Spergel, D., Gehrels, N., Baltay, C., et al. 2015, ArXiv e-prints [arXiv:1503.03757]
Sullivan, M., Ellis, R. S., Howell, D. A., et al. 2009, ApJ, 693, L76
Sullivan, M., Conley, A., Howell, D. A., et al. 2010, MNRAS, 406, 782
Suzuki, N., Rubin, D., Lidman, C., et al. 2012, ApJ, 746, 85
Thielemann, F.-K., Nomoto, K., & Yokoi, K. 1986, A&A, 158, 17
Timmes, F. X., Brown, E. F., & Truran, J. W. 2003, ApJ, 590, L83
Wang, X., Li, W., Filippenko, A. V., et al. 2009, ApJ, 697, 380
Zahid, H. J., Bresolin, F., Kewley, L. J., Coil, A. L., & Davé, R. 2012, ApJ, 750, 120